Caving 2022 - Y Potvin (ed.)

doi:10.36487/ACG_repo/2205_50

Surface subsidence analysis associated with caving at La Encantada Silver Mine

TV Garza-Cruz *Itasca Consulting Group, Inc., USA*

E Ghazvinian *Itasca Consulting Group, Inc., USA*

MA Fuenzalida *Itasca Consulting Group, Inc., USA*

ME Pierce *Pierce Engineering, USA*

E Ledesma *La Encantada Silver Mine, Mexico*

Abstract

This study describes a multi-year effort to calibrate a numerical model to mapped surface subsidence and other damage indicators in a historic silver mine that is now being exploited via caving. In 2017, the subsidence extent along with the general condition and character of the rock mass both underground and in the vicinity of the craters was evaluated during a site visit. Surface cracks were mapped in the vicinity of the existing crater to provide a more accurate representation of the 2017 fracture limit that needed to be captured by the numerical model before any forward prediction was made. A numerical model was developed to back analyse the 2017 conditions following from the historic mining that had taken place, resulting in close agreement with observations made on site. A forward surface subsidence prediction was then obtained based on the target draw schedule to exploit the remaining orebody via caving. In 2020, the actual draw schedule followed until that point was updated in the model to evaluate the validity of the results of the numerical model as well as future predictions. As new extraction points with updated production tonnages were added to the mining plan, the calibrated model was used to provide updated estimates of cave growth, surface subsidence, and building/infrastructure potential damage through the life-of-mine.

Keywords: *subsidence, caving, surface infrastructure stability, numerical modelling*

1 Introduction

La Encantada Silver Mine, owned and operated by First Majestic Silver Corp., is located in northern Mexico, 708 km northeast of Torreon, Coahuila. The previous mine operator employed post pillar cut-and-fill, with rock backfill containing a higher grade than the current mining cut-off grade. Therefore, the mine wanted to exploit the higher-grade ore that was left as pillars, as well as the economical backfill materials from the La Prieta mining zone using a hybrid mining method including incline caving and block caving (Boutilier et al. 2019; Herrera et al. 2019).

The historic mining activities at the upper level of the old La Prieta and Escondida mining zones by the previous mine operators resulted in two surface subsidence zones above the La Prieta mining zone.

Records of tonnages mined by the previous operator are not available. Therefore, historic mining has been estimated for the purpose of this study primarily based on old maps of development. This lack of information poses a challenge in the ability to model the pre-caving conditions at the La Prieta area, since two craters and a surrounding fractured zone currently exist as a result of historic mining.

This paper describes a multi-year effort to calibrate a numerical model to the mapped surface subsidence in 2017 prior to the adoption of caving, followed by a forward prediction that was then re-evaluated in 2020 using the actual draw scheduled adopted until that point to generate a new prediction into the future.

2 Pre-caving surface subsidence (2017)

In 2017 two of the authors visited La Encantada Mine with the purpose of evaluating the pre-caving subsidence extent along with the general condition and character of the rock mass both underground and in the vicinity of the craters. During the site visit, surface cracks were mapped in the La Prieta area to provide a more accurate representation of the pre-caving fracture limit that needed to be captured by the numerical model before any forward prediction was made. The intention of the survey was to find the edge of visible cracks farthest from the crater. Figure 1 shows a satellite view of the La Prieta and La Escondida craters from Google Earth taken in 2014 with the mapped cracks superimposed. Pictures of selected mapped cracks can be found in Figure 2. The survey also revealed the damaged state of the rock forming the bridge between the La Prieta and La Escondida craters as shown in Figure 3. This is relevant, as it suggests that there are other historically mined areas besides the ones vertically down from the craters that may be contributing to the subsidence. The site visit also allowed the opportunity to access the La Escondida crater from underground. Figure 4 shows the rock fragments inside the crater as well as the sub-vertical walls forming it. Upon inspection of the crater walls, some sub-horizontal joints were readily visible in the limestone, which are expected to contribute to the good caveability of the La Prieta cave.

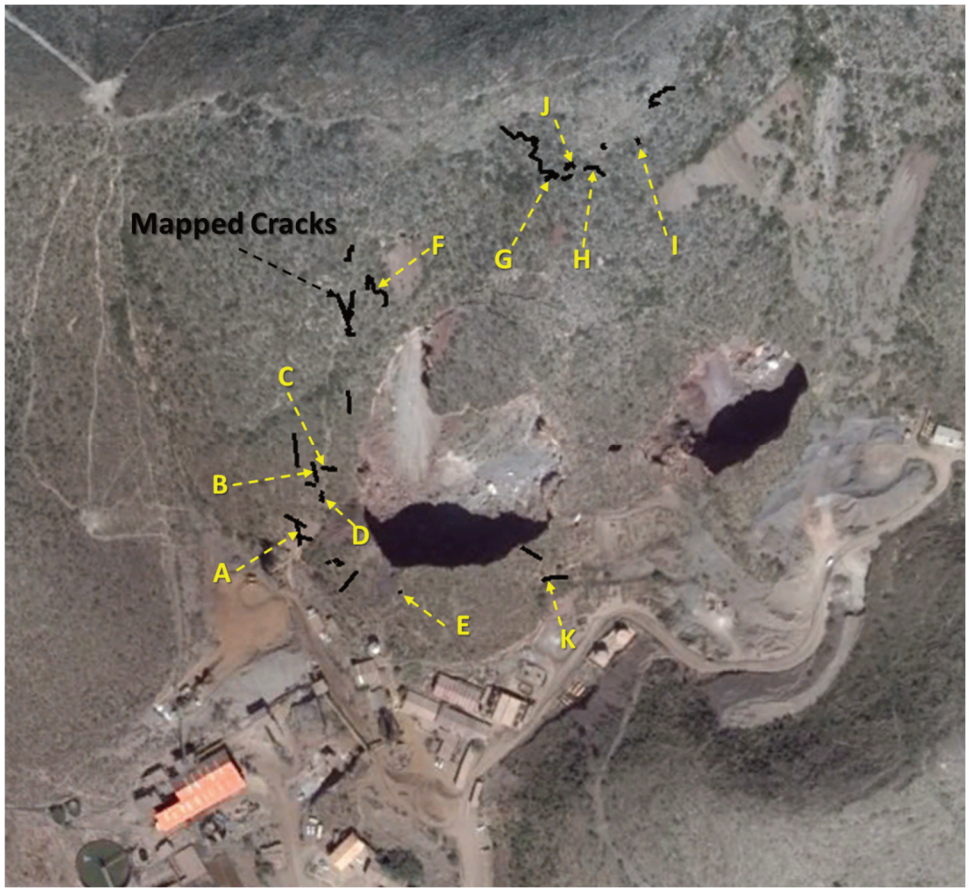

Figure 1 Satellite view of the La Prieta and La Escondida craters from Google Earth taken in 2014. The black lines correspond to the cracks mapped during the site visit. Letters denote the location of images taken during crack mapping as shown in Figure 2

Figure 2 Images of the cracks mapped during the site visit. The different letters correspond to the locations marked in Figure 1

Figure 3 Current state of the rock mass forming the bridge between the La Prieta and La Escondida craters. La Escondida crater is shown on the right

Figure 4 Fragmented rock inside the La Escondida crater. Crater walls are sub-vertical

3 Numerical approach to analysis of caving and subsidence

A large-scale FLAC3D (Itasca 2019) model that conformed with the topography was constructed to simulate the regional extent of the La Prieta operation. The faults were incorporated into the model as regions of weaker and softer material. The in situ stress regime needed to be assumed since no stress measurements were available. The vertical stress was assumed to be lithostatic (overburden weight), and a horizontal-to-vertical stress ratio of one (K0 = 1) was assumed in all simulations performed in this study.

3.1 Constitutive model

The Itasca Model for Advanced Strain Softening (IMASS) constitutive model (Ghazvinian et al. 2020b) was used in this study. IMASS is Itasca's most advanced strain softening model for simulation of rock mass response to mining. This model contains a two-stage softening behaviour as shown in Figure 5. The Hoek–Brown parameters of the residual strength envelopes are selected to approximate shear strength for rockfill material as defined by Barton & Kjaernsli (1981):

$$\tau = \sigma_n \tan\left(R.\log\left(\frac{S}{\sigma_n}\right) + \emptyset_b\right) \quad (1)$$

where τ is shear strength, σ_n is the normal stress, R is equivalent roughness (Figure 6), S is the rock block strength, and $\emptyset_b$ is the basic friction angle for the rock.

The first residual envelope (blue line) represents the mobilised post-peak strength. At this point, the rock mass is assumed to have undergone fracturing, but the resulting rock fragments are still fully interlocked. Consequently, porosity is considered to be close to zero. The second residual envelope (green line) represents the ultimate rock mass residual strength at the point of maximum bulking. At this point, the degree of rock fragment interlock is at its minimum, and the porosity is maximised (maximum porosity of 40% is assumed). Ideally, the first and second residual envelopes describe the behaviour of cohesionless, perfectly frictional material with different degrees of interlocking. The Hoek–Brown approximation of Equation 1 that is implemented in IMASS assumes the formation and interaction of very sharp, angular, and very rough

fragments during the course of bulking, from porosity of 0% to 40% on the Barton & Kjaernsli (1981) nomogram in Figure 6 (shown with the dashed red line).

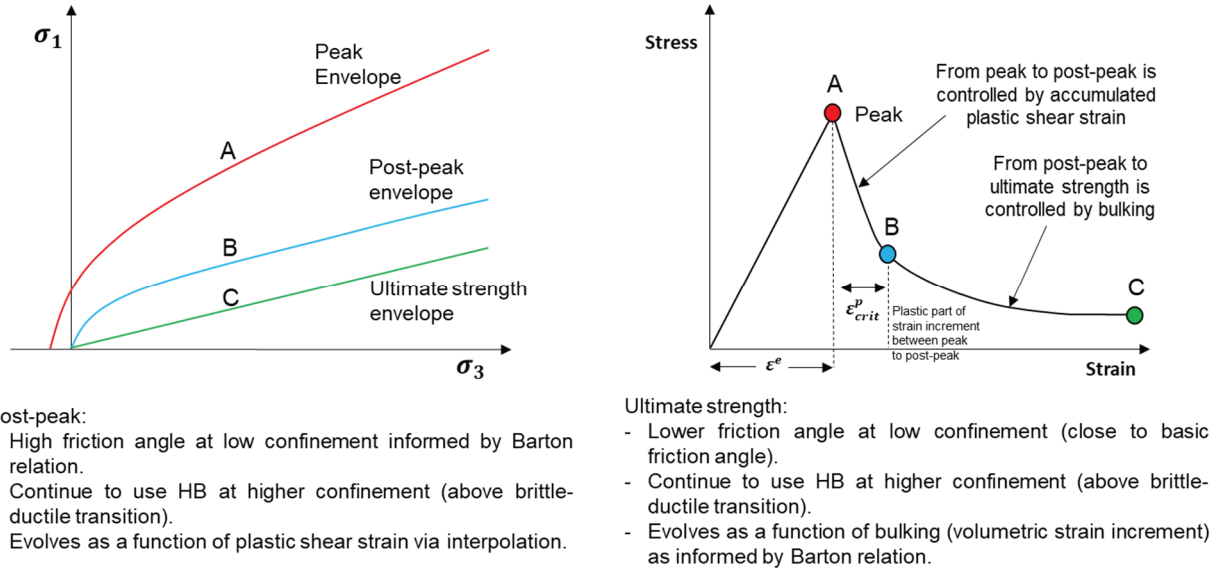

Post-peak:
- High friction angle at low confinement informed by Barton relation.
- Continue to use HB at higher confinement (above brittle-ductile transition).
- Evolves as a function of plastic shear strain via interpolation.

Ultimate strength:
- Lower friction angle at low confinement (close to basic friction angle).
- Continue to use HB at higher confinement (above brittle-ductile transition).
- Evolves as a function of bulking (volumetric strain increment) as informed by Barton relation.

Figure 5 Yield surfaces and material response for IMASS model

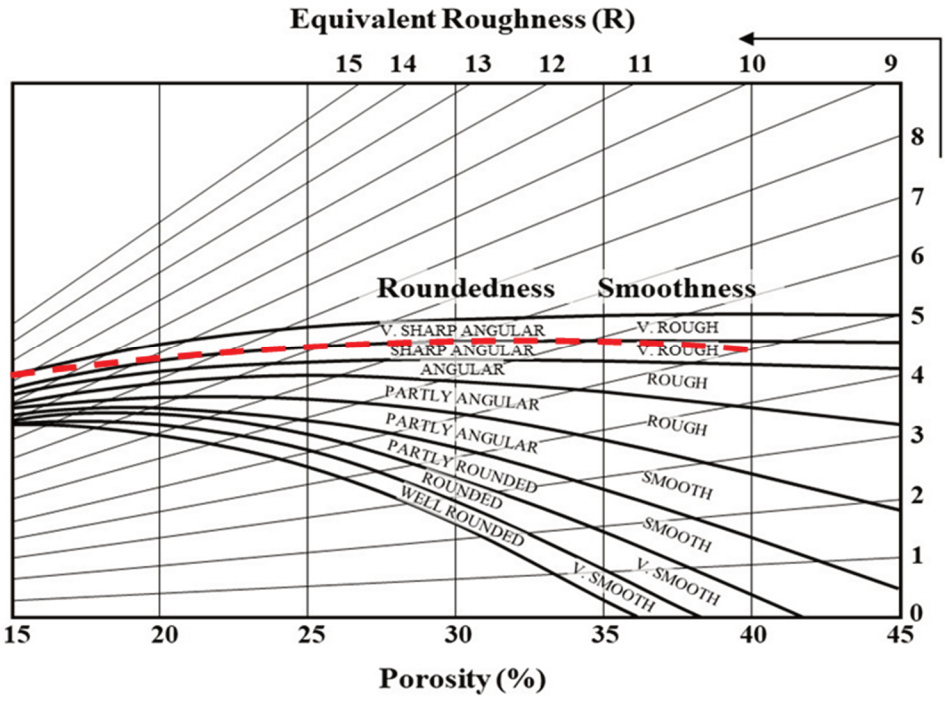

Figure 6 Equivalent roughness of an assembly of rock fragments based on porosity and fragment roundedness/smoothness (Barton & Kjaernsli 1981)

3.2 Rock mass properties

The rock mass properties used in the analysis are summarised in Table 1. Rock mass residual properties for all the units as used by IMASS are listed in Table 2.

Table 1 Rock mass properties used for the analysis

Unit	Density (kg/m^3)	GSI	mi	UCS (MPa)	Ei (GPa)
Cuerpo La Prieta	2,900	42	17.7	102.0	6.35
Cuerpo 660	2,700	35	7.0	25.0	1.50
Limestone	2,750	38	12.0	35.0	26.00
Skarn	3,050	68	29.0	250.0	16.90
Bx. Maria Isabel	2,700	22	17.0	30.0	24.00
Faults	Taken from host rock	20	8.5	17.8	Taken from host rock

Table 2 Rock mass residual properties

Unit	IMASS residual 1			IMASS residual 2			Max. bulking
	H–B m	H–B a	H–B s	H–B m	H–B a	H–B s	
All lithologies and faults	2.0	0.6	0	2.0	0.85	0	0.66 (~40% porosity)

4 Mining-induced subsidence

Mining-induced subsidence may put mine infrastructure at risk, while changes in the surface landscape may be dramatic and, in some cases, can lead to high environmental impacts. Therefore, the ability to predict surface subsidence has become increasingly important for operational risk and environmental impact assessment. The term subsidence used in this paper encompasses a wide range of surface effects associated with caving and not just the vertical displacement of the surface.

Mining-induced surface subsidence is typically characterised by three key zones: 1) the crater (often derived from the mobilised zone); 2) the fractured zone; and 3) the zone of continuous subsidence. The limits and shapes of these zones are mainly controlled by the overburden lithology spatial distribution and its associated rock mass strength, in situ stress, the presence of major structures, preferred joint orientations, topography, and footprint depth and shape.

Empirical models are widely used in early stages of mine design to describe the possible ground response as a consequence of mining based on observations and experience of actual mining subsidence. However, few guidelines exist for estimating the impact of the level of subsidence on infrastructure, particularly for more realistic three-dimensional footprint layouts. This becomes even more complicated in cases like the one studied here, where the historical number and location of tons produced is unknown. As noted by Flores & Karzulovic (2002), only numerical models allow the full extent of the influence zone to be predicted.

4.1 Fracture limit

The large-scale surface cracking (fractured) zone consists of an area around the crater in which the ground surface is broken and has open tension cracks, benches, and rotational blocks. The outer limit of this zone is called the fracture limit. The primary failure mechanism associated with this zone is shear failure of the side rock. Other types of failure mechanisms, such as toppling and block rotation, are also present, but they appear to be secondary mechanisms that form after the primary shear failure develops. Another failure mechanism is tension failure, which manifests as tension cracks.

Back-analysis of the fracturing limits induced by caving at El Teniente mine conducted by Cavieres et al. (2003) showed that a total strain criterion of 5e-3 is a good indicator for delineation of the fracture zone limit from numerical modeling results. This criterion has been used extensively and has been validated further through back-analysis of fracture limits at Kiruna (Sainsbury & Stockel 2012), Grace (Sainsbury & Lorig 2005), Century Mines (Sainsbury et al. 2016), and Cadia East (Ghazvinian et al. 2020a) as well as Andina, Venetia, Lac des Isles, and Pampa Escondida (confidential reports).

4.2 Limit of continuous subsidence and building damage criterion

The continuous subsidence zone lies beyond the fracture limit and is where movement of the ground surface occurs without associated visible fracturing. The outer limit of this zone, corresponding to the location of zero subsidence, is not as well defined as the fracture limit because delineation in practice is a function of the precision of the monitoring system used. Rather than using thresholds of vertical or horizontal displacement to define this limit, the International Caving Study (Flores & Karzulovic 2004) and the Society of Mining Engineers (SME 2011) recommend adopting strain thresholds to define the limits of the continuous zone that are based on site-specific acceptability criteria. Most often, the strain thresholds adopted to define the limit of continuous subsidence are based on empirical criteria for damage to buildings, as masonry-founded structures tend to be sensitive to both horizontal strain and angular distortion. They are more sensitive to such strains than rock masses, which are typically jointed and therefore capable of sustaining higher strains without fracturing. This explains why the strain limits for cracking of masonry foundations generally lie farther out from the cave crater than the rock mass fracture limit.

A major concern during the planning and execution of underground mining is the impact of ground movements on adjacent buildings and utilities. One aim of defining the subsidence zones is to assess stand-off distances for the sitting of mine shafts, excavations, and other infrastructure.

Vertical displacements alone cause little damage to surface infrastructure (Peng 1999). Singh (2003) provides examples of an observation tower that sank 30 ft (9.2 m) in a coalfield, mining structures that subsided a similar amount around the sulfur mining areas off the coast of Louisiana, and a church in a potash-mining district that settled 20 ft (6.2 m), all without significant damage. Uniform horizontal movements of the ground surface also cause little damage to structures, although breaks in pipes, electric or communications lines, roads, and other features may occur. Tilt also may not cause damage but can change the gradients of railroad tracks and highways, and cause tanks to overflow and interfere with gravity drainage. The limits of subsidence associated with cave mining are normally related to strain (rather than displacement), as surface horizontal strains cause most of the damage to the rock mass and surface infrastructure surrounding mined areas.

The concept of tolerable damage has led to the development of classification schemes for building damage (Harrison 2011). Boscardin & Cording (1989) developed a method for estimating potential building response to nearby excavation and compared their estimations with field data. In addition, Boscardin and Cording established a set of curves relating horizontal strain, angular distortion, and degree of cracking damage for brick-bearing wall structures that was then adapted by Harrison (2011) (Figure 7) to predict the degree of cracking in bearing-wall and small-frame structures adjacent to excavations, and compared with existing field measurements.

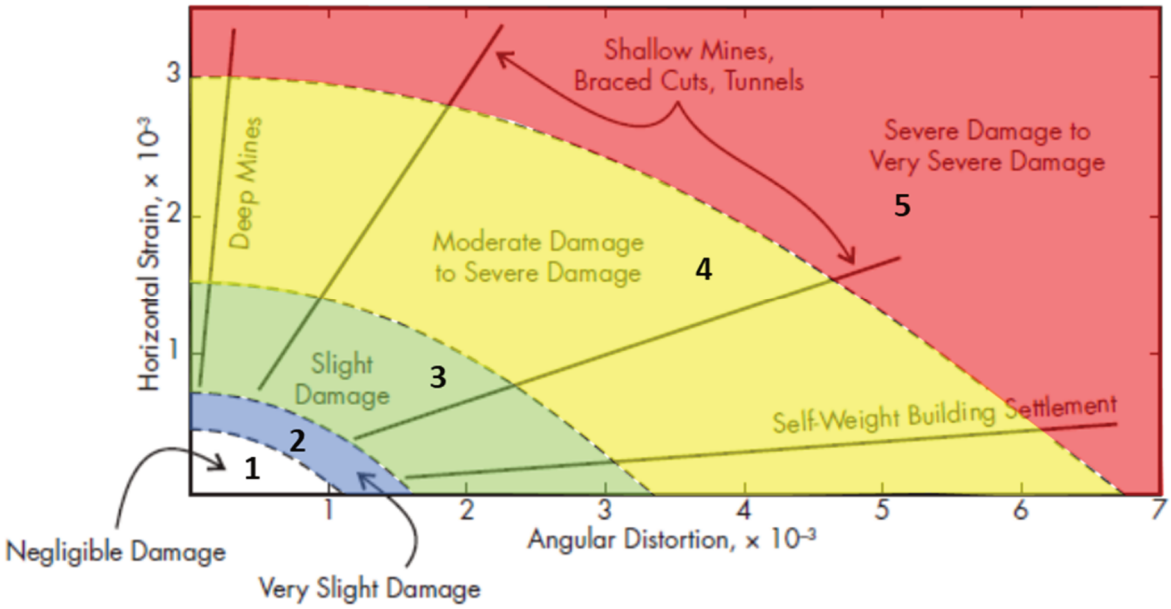

Figure 7 Building damage in terms of angular distortion and horizontal strain (modified after Harrison 2011)

The building damage criteria shown in Figure 7 are used in the present study to categorise the current and future potential building damage as a result of mining at La Encantada Silver Mine.

Throughout this document, the mobilised zone is defined as a region with vertical displacement exceeding 2 m. The fractured zone is defined as a region with the total measure of strain exceeding 0.5% and is used to demarcate the limits of visible fracturing that would be expected from mining. The fractured zone limit also coincides with the edge of the severe to very severe damage (boundary between regions 4 and 5 in Figure 7) in the building damage criterion.

5 Model calibration to pre-caving conditions

As previously mentioned, records of tonnages mined by the previous operator are not available. This imposes uncertainty in terms of the extent of mining in the orebodies and the associated tonnages extracted. The information available for model calibration up to the 2017 conditions is as follows:

- Limits of the fractured zone based on the mapped surface cracks by the authors.
- Tight fractures mapped in the hoist room and sinkhole associated with the old workings and west stopes.
- The edge of the fracture zone in the tunnel access at level 1720 at an approximate distance of 30 m from the San Francisco shaft.
- Negligible damage on the mine office building.
- No indications of instability or damage in the Maria Isabel shaft.

Figure 8 shows the orebodies and mine developments converted to broken rock (with porosity ~40%) in terms of material properties during simulation of historical mining. The stresses within the mined areas were reset to zero in an iterative process to simulate historical mining until a good match between the model results and field observations was achieved.

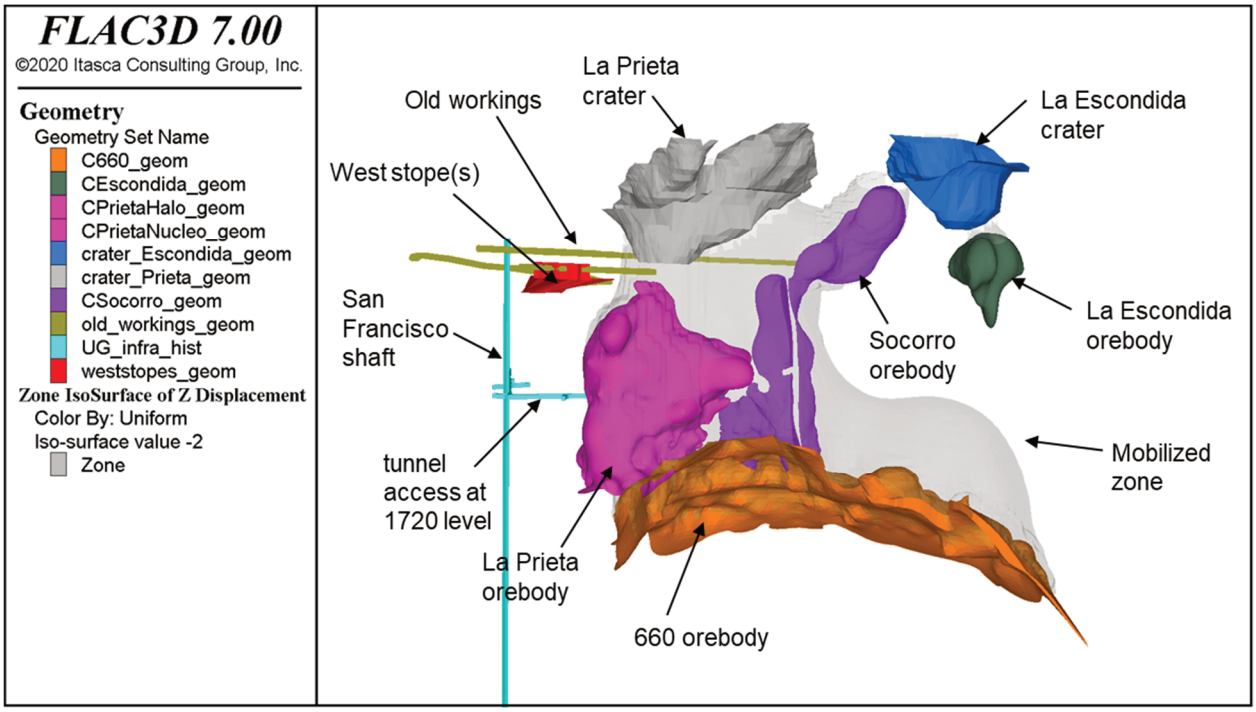

Figure 8 Orebodies and mine developments that were converted to broken rock to simulate historical mining and the corresponding mobilised zone

The fracture limit and building damage categories at ground surface after simulation of historical mining are shown in Figure 9 in plan view, representing the pre-caving surface subsidence conditions in 2017. The fracture limit (black line) is observed to match closely with the surface cracks mapped by the authors (pink lines). In addition, the model results suggest that the office buildings are experiencing very slight to slight damage, which is consistent with the lack of damage reported by the mine.

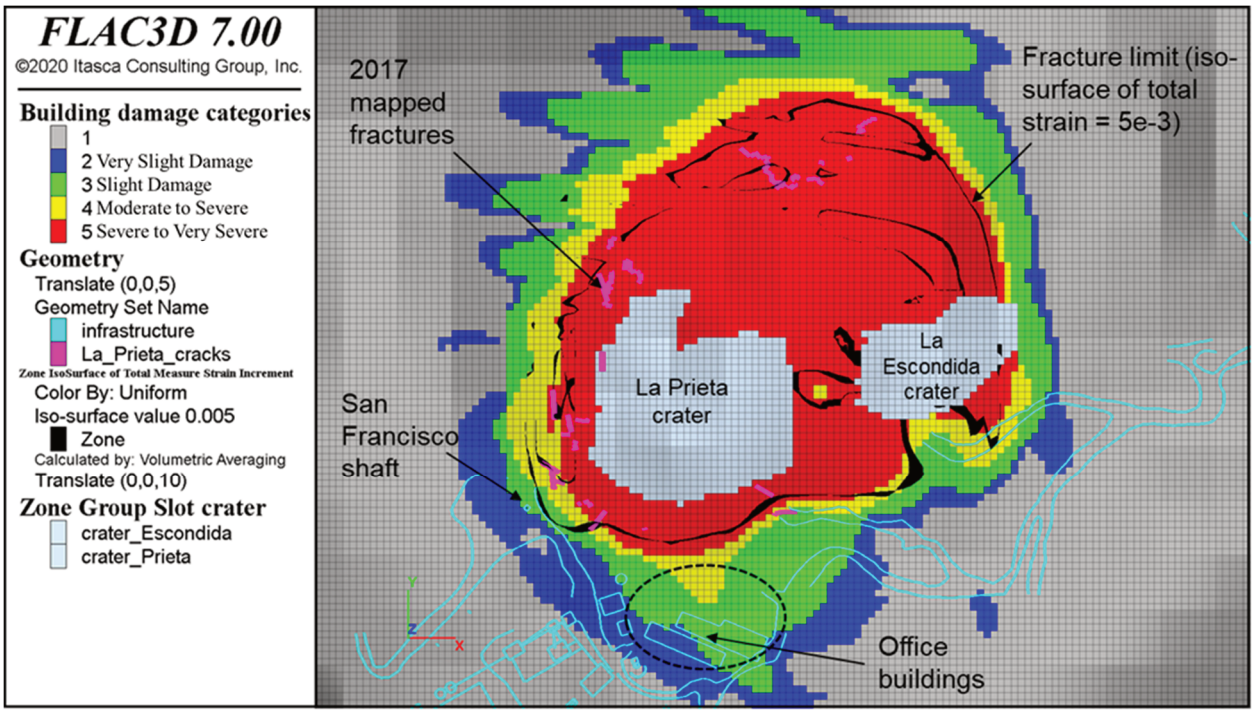

Figure 9 Fracture limit and building damage categories after simulation of historic mining (pre-caving)

A closer look at the fracture limit in the southwest corner of the La Prieta crater is shown in Figure 10 and Figure 11. In Figure 10, where the wireframe of the hoist room and old workings are translated to the surface for reference, it can be seen that the fracture limit extends far enough to encompass the sinkhole mapped in 2018 (attributed by mine personnel to historic mining and the presence of old workings). Including historic mining of the west stopes was critical in capturing this. Figure 11 shows how ore extraction from the west stopes has locally influenced the extension of the fracture limit. The hoist room is located directly above the west stopes and is affected by the locally extended fracture limit. This explains the tight fractures mapped in the hoist room prior to the recent mining.

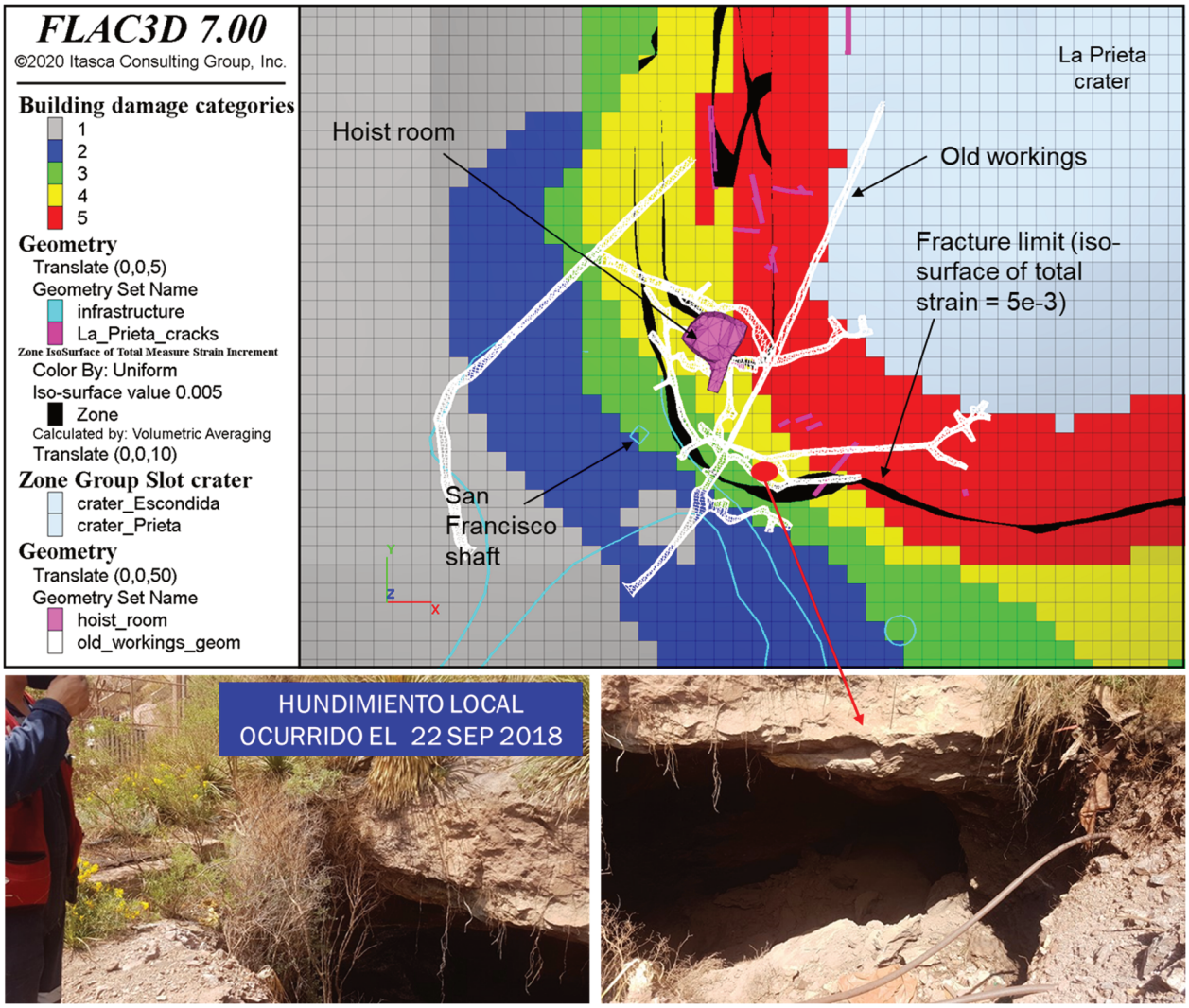

Figure 10 Detailed look at the fracture limit in the southwest corner of the La Prieta crater and the location of observed sinkhole in 2018

In terms of fracture limit at depth, Figure 12 shows the evolution of the fracture limit in the vicinity of the mined orebodies after historic mining. The edge of the fracture limit along the tunnel access at the 1720 level is predicted by the model to extend to a distance approximately 35 m from the San Francisco shaft, which is in close agreement with the 30 m measured by the mine.

The close agreement between the calibrated model results in terms of emergent surface subsidence, fracture limit, and building damage (or lack thereof) relative to all the available field observations increases the confidence in the assumptions and was taken as a positive indication of the model being sufficiently calibrated to be used in forward predictions.

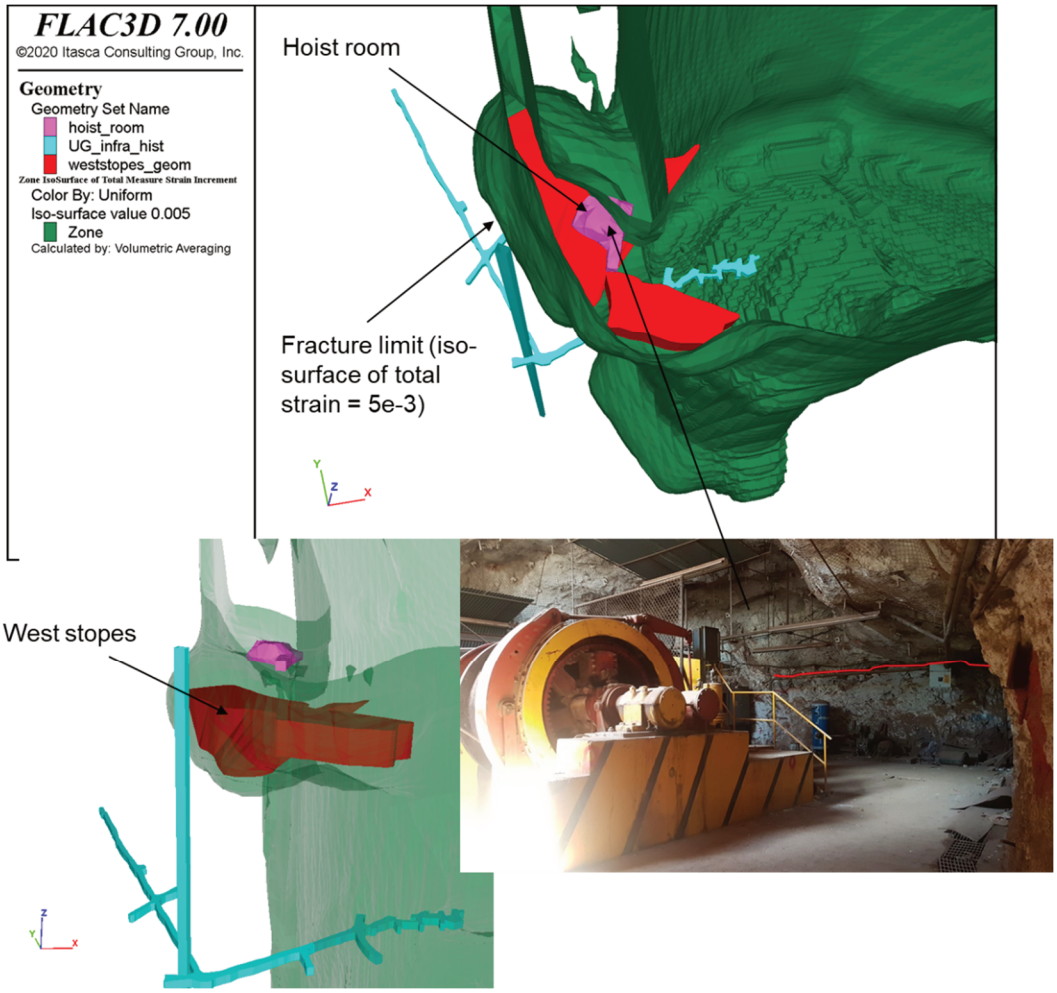

Figure 11 Tight fractures mapped in the hoist room in 2018 and the relative location of the hoist room with respect to west stopes

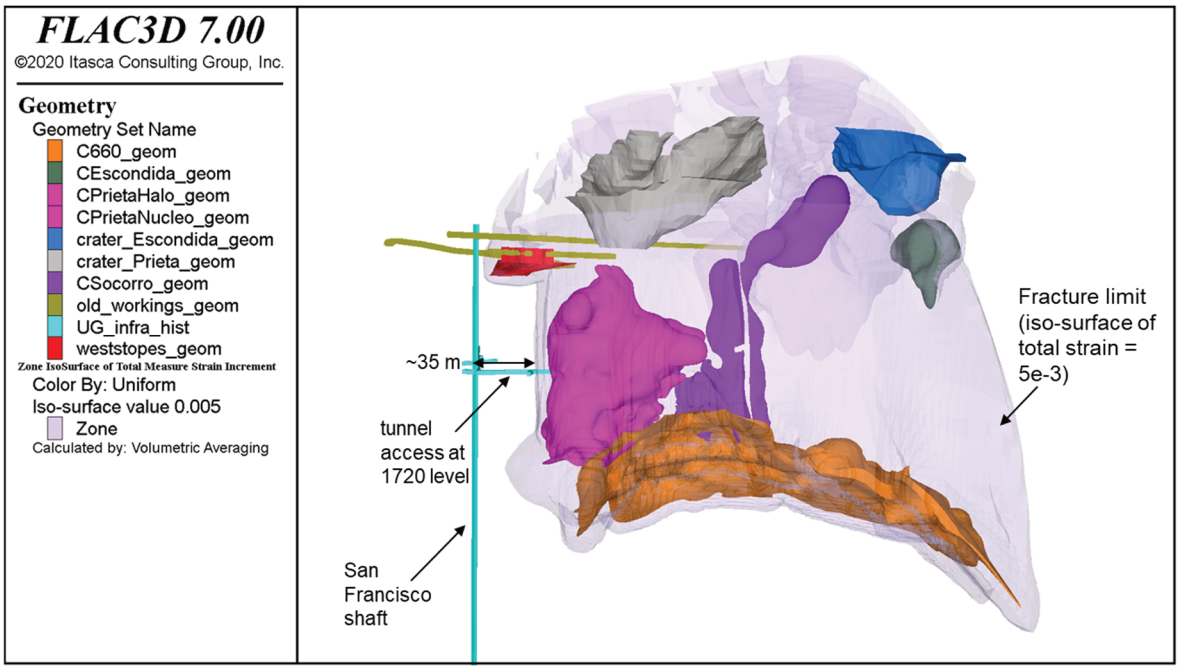

Figure 12 Fracture limit in the vicinity of the mined orebodies after historic mining (pre-caving)

6 Predictions of surface subsidence

The calibrated model was used along with the planned mining rates to make a prediction of surface subsidence. As mining took place, a close agreement between the predictions and the actual surface subsidence experienced was reported by the mine. In 2020, after the mine had produced about 50% more tonnages than originally simulated, a model update was performed. Due to space limitations of the current paper, only the updated model along with the subsequent prediction is described next.

Simulation of production between October 2018 and September 2020 was performed using the Itasca caving algorithm. The reconciled tonnes for La Prieta and C660 during this period was used in the analysis. The available information for model calibration is as follows:

- Limits of the fractured zone based on mapped surface cracks (September and October 2020).
- Limits of the fractured zone based on the drone flyovers.
- Negligible damage on the mine office building (surveyed in 2020 by mine personnel).
- MPBX data.

The fracture limit and building damage categories after simulation of the 2018–2020 mining are shown in Figure 13, representing the surface subsidence conditions at the end of September 2020. Overall, the fracture limit encompasses all the mapped fractures by mine personnel and surveyed fractures from drone flyovers during recent mining. Interestingly, the southern and southwestern extent of the fracture limit coincides with some of the mapped fractures in October 2020 (marked by dashed circles), indicating that the model is not over-predicting the fracture limit. In addition, the model results suggest that the office buildings are experiencing very slight to slight damage, which is consistent with negligible damage reported by mine personnel in 2020.

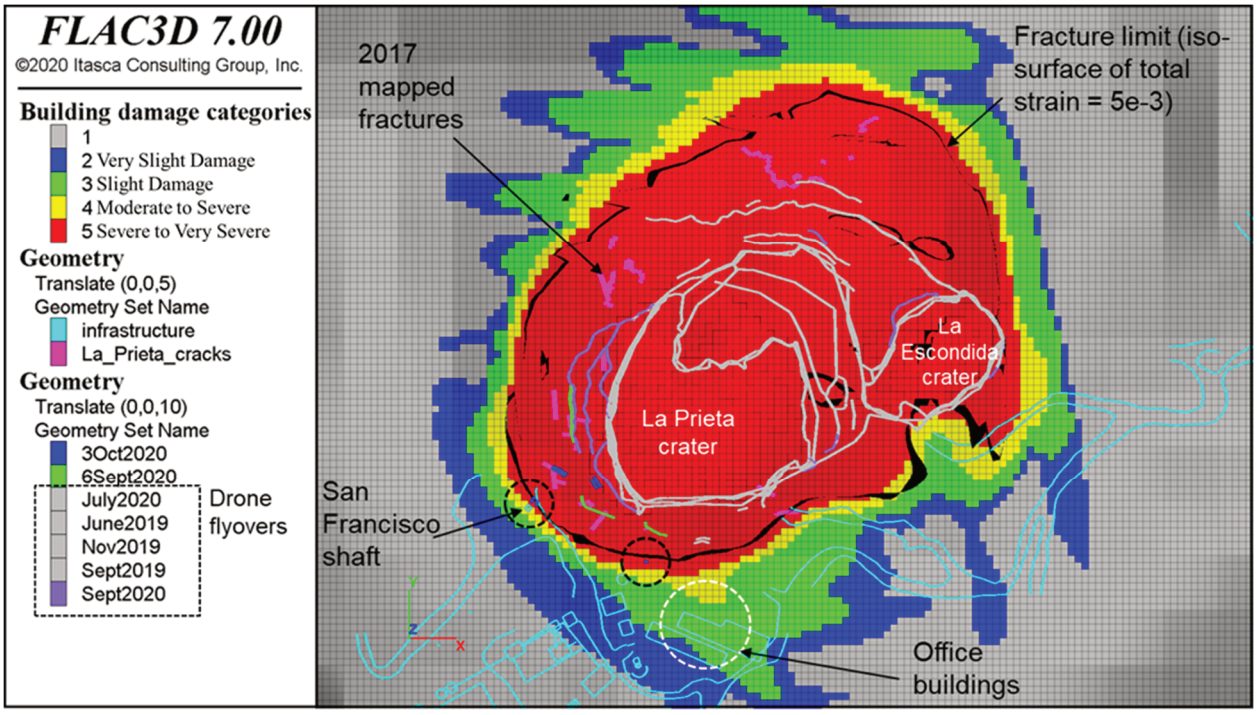

Figure 13 The fracture limit and building damage categories after simulation of 2018–2020 mining

The fracture limit has mainly grown to the south, west, and northwest of the La Prieta crater during the 2018–2020 production. The model results indicate that in the south, the fracture limit has grown between 10 and 15 m closer to the office buildings.

The close agreement between the model response to production during that period and field observation suggests that the model is reasonably calibrated and will provide a reliable forecast of subsidence as production continues.

An updated mine design and production schedule was implemented into the 2020 conditions model to assess the potential for additional surface subsidence and building damage through production from the remainder of the La Prieta and C660 orebodies as well as Ojuelas.

Figure 14 shows the evolution of the fracture limit between September 2020 through the completion of the planned mining. The extension of the fracture limit during this period evolves in the north, west, and south directions. Figure 15 shows the predicted mobilised limit at the end of the planned mining. Comparing this plot with the previously derived mobilised limit (September 2020) in Figure 13 suggests that the evolution of the fracture limit in the south and west are directly influenced by the mining of La Prieta and the western flank of C660, propagating the cave vertically up and extending the crater and the fracture limit to the south and the west. The propagation of the fracture limit to the north, on the other hand, is influenced by the relative location of the drawpoints with respect to the topography. The continuous production would undermine the upslope area, promoting gravity-driven movements to the north. No significant changes in terms of cratering or extension of fracture limit on the surface is expected due to mining of Ojuelas. The mobilised volume of the rock mass and the limits of the fractured zone associated with production from Ojuelas is expected to be encapsulated underground due to the relatively deep orebody and small ratio of draw height to mining footprint (Figure 15).

The model predicts that the fracture limit will increase in size on its southern edge towards the mine office building between 15 and 20 m by the time mining of La Prieta and C660 is completed. Similarly, the forecasted higher building damage categories will progressively grow towards the mine office building.

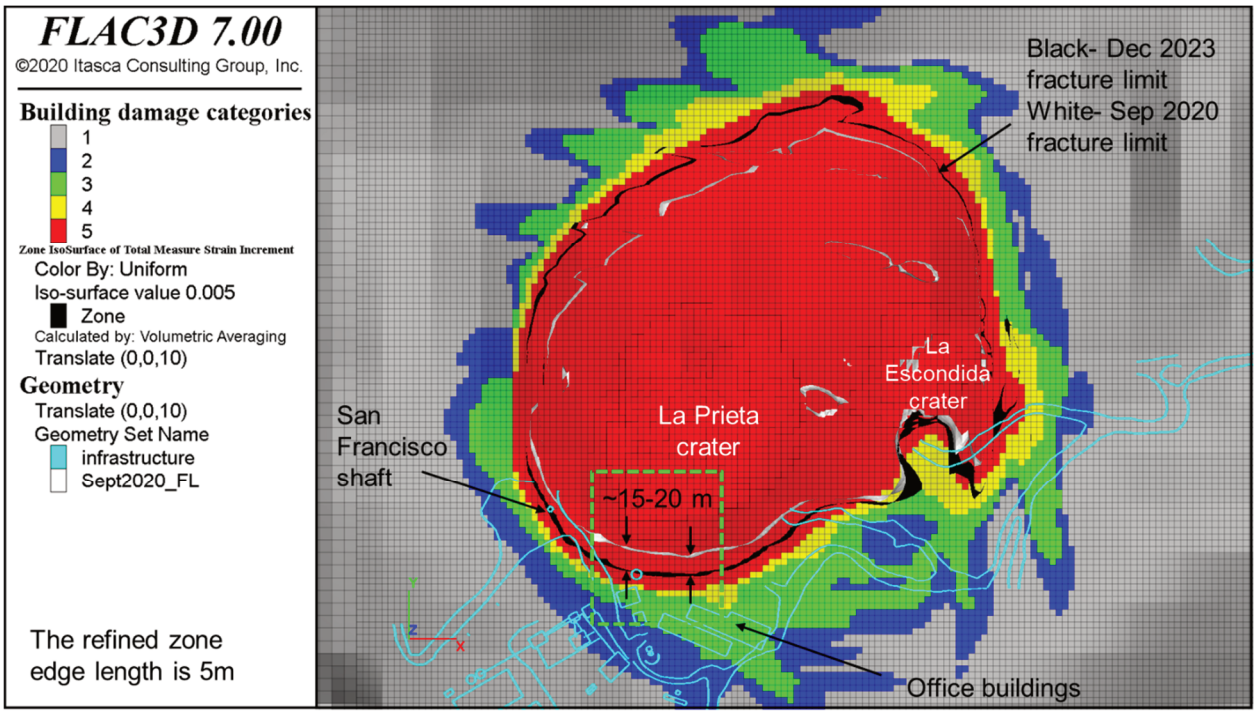

Figure 14 Predicted fracture limit and surface subsidence after completion of planned production from La Prieta and C660 orebodies

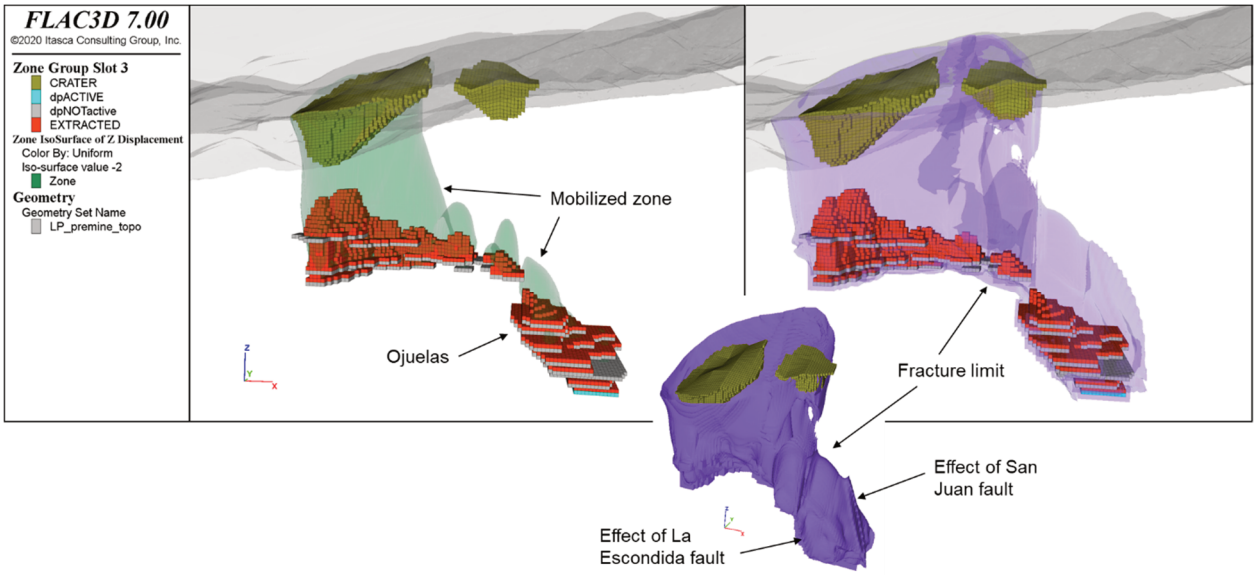

Figure 15 Predicted fracture limit and mobilised zone at the end of planned production

7 Conclusion

A numerical model has been developed to simulate the pre-caving conditions at La Prieta in La Encantada mine. The emergent results obtained are in close agreement with observations made on site. The results of the calibrated model pre-caving capture a tight and continuous fractured zone surrounding the La Prieta and La Escondida craters that matches well with the edge of mapped cracks on site. The model predicts the edge of the fracture zone at level 1720 to be at an approximate distance of 35 m from the San Francisco shaft, consistent with measurements by the mine. Additionally, the model suggests negligible to very slight damage on the mine office building along with no indications of instability or damage in the Maria Isabel or San Francisco shafts. All of this is in accordance with observations of pre-caving conditions. Therefore, this numerical model was deemed representative of the pre-caving conditions and used in a forward analysis by incorporating the proposed mining sequence and tonnages, with the objective to elucidate the potential impact caving would have on ground subsidence and building damage.

As mining took place, a close agreement between the predictions and the actual surface subsidence experienced was reported by the mine. In 2020, after the mine had produced about 50% more tonnages than originally simulated, a model update was performed along with a subsequent forecast.

With the planned production from La Prieta and C660 orebodies, the fracture limit is predicted to grow ~15–20 m in the south, ~5–20 m in the west, and to a larger extent in the north between October 2020 and the end of the simulated mining. This will put the fracture limit approximately 20 m from the office buildings.

The growth of the fracture limit in the south and in the west is directly associated with extraction of tonnage and vertical growth of the cave. The accelerated evolution of the fracture limit in the north, on the other hand, is due to a combination of high slope angle and production (undermining the upslope area). The extent of fracture limit and mobilised zone on the surface is not substantially affected by production from Ojuelas.

Acknowledgement

The authors acknowledge the La Encantada rock mechanics team for providing insights into the mine's ground behaviour, in addition to input data, and the First Majestic Silver Corp. management team for permission to publish this paper.

References

Barton, N & Kjaernsli, B 1981, 'Shear strength of rockfill', *Journal of Geotechnical and Geoenvironmental Engineering*, vol. 107, ASCE 16374.

Boscardin, MD & Cording, EJ 1989, 'Building response to excavation-induced settlement', *Journal of Geotechnical Engineering*, vol. 115, no. 1, pp. 1–21.

Boutilier, B, Sinuhaji, A & Mendoza, R 2019, 'The construction of two small-scale caving mines at La Encantada mine, Mexico', *Mining Engineering*, vol. 71, no. 9.

Cavieres, P, Gaete S, Lorig L & Gómez P 2003, 'Three-dimensional analysis of fracturing limits induced by large scale underground mining at El Teniente mine', in PJ Culligan, HH Einstein & AJ Whittle (eds), *Soil and Rock America 2003: Proceedings of the 39th U.S. Rock Mechanics Symposium*, Verlag Glückauf, Essen, pp. 893–900.

Flores, G & Karzulovic A 2004, *Geotechnical Guidelines for a Transition from Open Pit to Underground Mining: Subsidence*, report to International Caving Study II.

Ghazvinian, E, Fuenzalida M, Orrego C, & Pierce, M 2020a, 'Back analysis of cave propagation and subsidence at Cadia East Mine', in R Castro, F Báez & K Suzuki (eds), *MassMin 2020: Proceedings of the Eight International Conference and Exhibition on Mass* Mining, University of Chile, Santiago.

Ghazvinian, E, Garza-Cruz, T, Bouzeran, L, Fuenzalida, M, Cheng, Z, Cancino, C, & Pierce, M 2020b, 'Theory and implementation of the Itasca Model for Advanced Strain Softening (IMASS)', in R Castro, F Báez & K Suzuki (eds), *MassMin 2020: Proceedings of the Eight International Conference and Exhibition on Mass* Mining, University of Chile, Santiago, pp. 451–461.

Harrison, JP 2011, 'Mine subsidence', *SME Mining Engineering Handbook*, 3rd edn, Society for Mining, Metallurgy & Exploration, Englewood.

Herrera, G, Negrete, D, Sinuhaji, A & Reyes, RM 2019, 'Support elements and monitoring design for the San Javier breccia sublevel caving mine at La Encantada Silver Mine', *SME Annual Conference & Expo and CMA 121st National Western Mining Conference*.

Itasca Consulting Group, Inc. 2019, *FLAC3D – Fast Lagrangian Analysis of Continua in Three Dimensions*, version 7.0, computer software, Itasca Consulting Group, Inc., Minneapolis, http://www.itascacg.com/software/FLAC3D

Peng, S S 1999, *Surface Subsidence Engineering*, Society for Mining, Metallurgy & Exploration, Englewood.

Sainsbury, D & Lorig L 2005, *Investigation of Mining-Induced Subsidence at the Abandoned Grace Mine*, report to New Morgan Properties, L.P., Ref. ICG04-2262-29, Itasca Consulting Group, Inc., Minneapolis.

Sainsbury, B & Stockel, BM 2012, 'Large-scale caving and subsidence assessment at the Kiirunavaara lake orebody', *MassMin 2012: Proceedings of the 6th International Conference & Exhibition on Mass Mining*, Canadian Institute of Mining, Metallurgy and Petroleum, Montreal, pp. 243–253

Sainsbury, DP, Sainsbury, BL & Sweeney, E 2016, 'Three-dimensional analysis of complex anisotropic slope instability at MMG's Century Mine', *Mining Technology*, vol. 125, no. 4, pp. 212–225.

Singh, MM 2003, 'Mine subsidence', *SME Mining Engineering Handbook*, 3rd edn, Society for Mining, Metallurgy & Exploration, Englewood.

SME 2011, *SME Mining Engineering Handbook*, 3rd edn, Society for Mining, Metallurgy & Exploration, Englewood.